Mehmet Bozca[1], *Tatjana Lazović*[2*], *Pavle Ljubojević*[2], *Jovana Antić*[2]

ESTIMATION OF ROLLER BEARING SERVICE LIFE USING COMPUTATIONAL MODELLING

PROCENA RADNOG VEKA CILINDRIČNO-VALJČANIH LEŽAJA PRIMENOM RAČUNARSKOG MODELIRANJA

Originalni naučni rad / Original scientific paper
Rad primljen / Paper received: 23.02.2026
https://doi.org/10.69644/ivk-2026-siA-0087

Adresa autora / Author's address:
[1)] Yildiz Technical University, Mechanical Engineering Faculty, Istanbul, Turkey M. Bozca https://orcid.org/0000-0002-2620-6053

[2)] University of Belgrade, Faculty of Mechanical Engineering, Belgrade, Serbia T. Lazović https://orcid.org/0000-0001-8919-3336 , *email: tlazovic@mas.bg.ac.rs ;
P. Ljubojević https://orcid.org/0000-0002-5546-5046 ;
J. Antić https://orcid.org/0009-0002-6452-0294

Keywords

- roller bearing
- contact pressure
- Von Mises stress
- Basquin's equation
- fatigue life

Abstract

Service life is the period during which a rolling bearing operates under cyclic contact loading before failure due to fatigue occurs. In roller bearings, repeated line contact induces alternating subsurface shear stresses, making fatigue one of the most critical failure mechanisms under practical service conditions. Accurate fatigue life prediction is therefore essential for reliable bearing design and operation. This study investigates the fatigue behaviour of roller bearings by analysing the influence of contact-induced stresses, material properties, and operating conditions on bearing service life. A numerical modelling framework based on rolling contact fatigue principles and Hertzian contact theory is employed to evaluate stress distributions within bearing components. The analysis covers key design parameters, including roller geometry and elastic material properties, together with representative loading conditions. The results define a range of design parameters and service conditions that contribute to reduced contact stresses and increased fatigue life of roller bearings, providing a basis for improved bearing design and more reliable life prediction.

Ključne reči

- cilindrično-valjčani kotrljajni ležaji
- kontaktni pritisak
- Von Misesov napon
- Baskinova jednačina
- zamorni vek

Izvod

Radni vek je period tokom kojeg kotrljajni ležaj radi pod cikličnim kontaktnim opterećenjem pre nego što dođe do otkaza usled zamora. Kod cilindrično-valjčanih ležaja, podpovršinski zamor je jedan od najkritičnijih mehanizama otkaza u realnim eksploatacionim uslovima. Zbog toga je tačna procena zamornog veka od suštinskog značaja za pouzdano konstruisanje i rad ležaja. U ovom radu analizira uticaj kontaktnih napona, svojstava materijala i radnih uslova na vek ležaja. Numerički okvir modeliranja, zasnovan na principima zamora kotrljajnog kontakta i na Hercovoj teoriji kontakta, primenjen je za određivanje raspodele napona u delovima ležaja (valjčići i staze kotrljajnih prstenova). Analiza obuhvata ključne konstrukcione parametre, uključujući geometriju valjčića i elastična svojstva materijala, zajedno sa odgovarajućim uslovima opterećenja. Rezultati definišu opseg konstrukcionih parametara i radnih uslova koji doprinose smanjenju kontaktnih napona i povećanju zamornog veka cilindrično-valjčanih ležaja, čime se obezbeđuje osnova za unapređeno projektovanje i pouzdaniju procenu radnog veka.

INTRODUCTION

Rolling bearings are widely used in rotating machinery, as they are designed to provide high efficiency, compactness, and the ability to support loads under various operating conditions. As critical components of mechanical systems, their performance and service life have a significant impact on overall machine reliability, since bearing failure often leads to partial or complete system failure /1-3/. During the bearing selection process, designers are required to estimate the bearing service life in terms of operating time or number of revolutions for a specified level of reliability. Provided that the bearing is correctly selected, transported, stored, installed, operated within the prescribed load and speed limits, and properly maintained through adequate lubrication and effective protection against contaminants, fatigue remains the dominant damage mechanism governing bearing life, /4/. Standardisation is one of the advantages of rolling bearings /5/. The formulation used for bearing service life estimation has been continuously developed and validated through standardisation for more than a century; however, it still does not account for all influential factors affecting bearing performance. Moreover, under certain operating conditions, the application of the standard life equation may result in inaccurate life predictions, leading either to oversized bearing designs or to premature failure before the predicted service life is reached. Consequently, further research is required in the field of rolling bearing life prediction, including the development of advanced mathematical models, their experimental validation, as well as numerical analyses and simulation-based approaches.

The parameters influencing fatigue failure and fatigue life in rolling bearings may be grouped into three main categories: geometric characteristics, material properties, and loading conditions. The adopted classification of these design-

related parameters is illustrated in Fig. 1. Within this classification, geometric parameters include the radii of the inner and outer raceways as well as the dimensions of the rolling elements, such as ball or roller radius and roller length. These parameters are primarily defined during the early design stage, based on shaft dimensions and the expected loading conditions. Material parameters comprise properties such as elastic modulus, Poisson's ratio, and material strength, which are selected by bearing designers and manufacturers in accordance with strength requirements and material availability. Loading parameters refer to factors such as transmitted power and operational load conditions, which are specified by the application requirements. In addition, lubrication conditions are typically recommended by the bearing manufacturer and adapted to the specific operating environment.

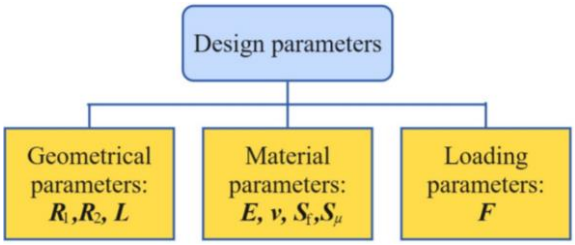


Figure 1. Design parameter classification for fatigue failure.

Lubrication behaviour is strongly influenced by operating temperature and the distribution of applied loads among the rolling elements /6, 7/. Previous studies show that elevated temperatures can lead to a reduction in the fatigue limit, an effect that has been incorporated into bearing life prediction models /8/. Moreover, strategies aimed at extending bearing service life through improved lubrication conditions have been comprehensively discussed in the literature /9/. Bearing fatigue failure may occur when the selected design and operating parameters are insufficient to satisfy the required working conditions. In practice, loading conditions often exceed their predicted values due to adverse or uncontrolled environmental influences.

The following studies focus on load-carrying capacity and fatigue life of rolling bearings based on Hertzian stress. According to a review on rolling contact fatigue in /9/, rolling contact fatigue occurs due to the removal of metallic particles from the surface of balls/rollers and/or raceways. Neglecting the lubrication effects, the bearing contact-stress is managed by Hertzian theory. Spalling, which is subsurface-originated and pitting, which is surface-originated, are the two dominant rolling contact fatigue events, /10/.

The fatigue behaviour of a double-row slewing ball bearing with non-uniform geometry is analysed in /11/. The authors report that, in contact-related problems, maximal stress levels are typically located beneath the surface rather than at the surface itself. Bearing fatigue life is evaluated using classical fatigue approaches, namely stress-life and strain-life concepts, with the number of cycles to failure determined through Basquin-type relationships derived from stress-life theory. In /12/, the load-carrying capability of the raceway in a three-row roller slewing bearing is examined. The study demonstrates that a logarithmic roller profile effectively mitigates edge contact stresses that are characteristic of cylindrical rollers. Although cylindrical rollers provide a larger nominal contact area, stress concentrations developing near the roller ends are shown to be detrimental to bearing performance. A numerical framework for evaluating both static load capacity and service life of large slewing bearing raceways is proposed in /13/. The results indicate that static load capacity assessment requires solving the bearing static equilibrium while simultaneously accounting for local contact conditions described by Hertzian contact theory. The static load capacity of a large double-row slewing ball bearing with predefined geometric irregularities is investigated in /14/. The adopted approach relies on Hertzian contact formulations, combined with vector-based algorithms to accurately represent the bearing geometry. In /15/, a computational methodology is introduced for estimating the dynamic load capacity of large three-row roller slewing bearings. The findings highlight that bearing clearance and deformation of the supporting rings play a crucial role in shaping the internal contact force distribution, thereby directly influencing the maximum contact forces. A further numerical study addressing the static load capacity of three-row roller slewing bearings with arbitrary clearances and predefined raceway geometries is presented in /16/. It is shown that an increase in axial clearance, together with axial structural deformation of at least one bearing ring, generally leads to a pronounced reduction in the bearing's static load capacity. Computational evaluation of the permissible static loading of a roller-slewing bearing case-hardened raceway is presented in /17/. It is concluded that there are significant differences between each roller type concerning the limit contact load. Additionally, the case depth of the raceway and the angle of slope are also influencing parameters.

Theoretical quantitative analysis of the internal clearance influence on the service life of a universally loaded deep groove ball bearing is presented in /18/. The service life of a rolling bearing is calculated using a standardised formula, based on the bearing's dynamic load rate, equivalent load, and the appropriate exponent, depending on the rolling elements' shape. In the standard calculation method, the expression of the service life does not explicitly take into account the internal clearance. However, the influence of clearance is calculated indirectly through the corresponding values of the equivalent dynamic load's parameters.

The numerical evaluation of the load-carrying capacity of large rolling bearings with hardened raceways is experimentally verified in /19/. The study emphasises that the service life of machine elements, including bearings, is frequently governed by crack propagation processes within the material. Repeated external contact loading induces cyclic shear stresses, while excessive loading conditions promote crack initiation along shear planes, ultimately leading to a reduction in bearing life. An elastic-plastic finite element-based rolling contact fatigue damage accumulation model is developed in /20/ to investigate early fatigue failure mechanisms in rolling bearings while accounting for surface integrity effects. The study demonstrates that surface roughness, residual stress, and hardness significantly influence fatigue damage evolution and that optimal surface integrity parameters exist for maximising bearing fatigue life. In /21/, a three-dimensional continuum damage mechanics-based model

is developed to investigate stress distribution, damage initiation, and defect evolution in rolling bearings under multiaxial fatigue loading. The model is validated by comparing predicted fatigue life with vibration-based experimental data under different loading conditions.

A bearing life prediction model incorporating both surface and subsurface tribological effects is presented in /22/. The proposed approach is based on rolling contact fatigue concepts, where bearing life is assessed using an equivalent stress located beneath the contact surface. In addition, the study highlights that contaminants and chemically aggressive lubricant additives increasingly contribute to surface-initiated damage, making such failures a prevalent issue in contemporary rolling bearing applications.

Theoretical analyses of point contact conditions relevant to ball bearing applications are reported in /23, 24/, with particular emphasis on the influence of bearing geometry and material properties on stress distribution. The results demonstrate that larger ball diameters lead to reduced contact stresses, whereas an increase in the elastic modulus results in higher stress levels within the bearing. Similarly, line contact conditions characteristic of roller bearing applications are examined theoretically in /24, 25/.

Previous research on rolling bearing fatigue life has addressed complex loading conditions by accounting for internal clearance, ring flexibility, misalignment, and non-Hertzian contact effects to improve life prediction accuracy, /26/. The influence of variable loading spectra and material parameters has also been investigated using advanced fatigue damage accumulation models, demonstrating improved predictive capability over classical approaches /27/. In addition, thermomechanical analyses have shown that temperature effects, clearance variation, and lubrication conditions significantly influence bearing fatigue life, particularly at high rotational speeds, /7/.

In recent years, the concept of remaining useful life (RUL) has gained increasing attention in rolling bearing research, driving numerous studies on predictive maintenance. Data-driven RUL approaches have been proposed, but variations in operating conditions and bearing characteristics often reduce prediction accuracy /28/, while reviews highlight the strengths and limitations of statistical, machine learning, and deep learning methods /29/. Hybrid frameworks and advanced signal processing techniques have further improved robustness and reliability under severe conditions /30, 31/. However, physics-based models that directly relate contact stresses, material properties, and operating conditions to fatigue life remain limited. This study addresses this gap by developing a numerical modelling approach for cylindrical roller bearings based on Hertzian contact theory and rolling contact fatigue principles, providing clear design and service parameter ranges for reliable life estimation.

SURFACE FAILURE - CALCULATION OF CONTACT PRESSURE AND STRESS

All the surface-failure modes in which there is relative motion between the surfaces are essentially pure sliding. When two surfaces are in pure rolling contact or are primarily rolling in combination with a small percentage of sliding, a different surface failure mechanism occurs, called surface fatigue, /32-36/.

The stresses introduced in two materials contacting a rolling interface are highly dependent on the geometry of the surfaces in contact, as well as on the loading conditions and material properties. Two special-geometry cases are simpler to analyse. These cases are called sphere-on-sphere contact or point contact and cylinder-on-cylinder contact or line contact, /32-36/.

If the load is such that the stress in the material is applied only below its yield point, the deflection in the contact patch will be elastic, and the material surface will return to its original curved geometry after passing through the contact patch. Resulting stresses in the contact patch are called contact stresses or Hertzian stresses. This causes a fatigue-loading situation that eventually leads to surface fatigue failure, /32-36/.

Cylindrical contact

The cylindrical contact or line contact type is common in machinery. Roller bearings are an application of cylindrical contact. The contacted cylinders can be both convex, one convex and one concave, or in the limit, a cylinder-on-plane. In all such contacts, there is the possibility of sliding as well as rolling at the interface. The presence of tangential sliding forces has a significant effect on the stresses compared to pure rolling. The case of two cylinders in pure rolling and a sliding component will be considered, /32-36/.

Contact pressure and contact patch in a cylindrical contact

When two cylinders roll together, their contact patch will be rectangular and referred to as a line contact, as shown in Fig. 2. The pressure distribution will be a semi-elliptical prism of half-width a. The contact pressure is a maximum $p_{\max}$ at the centre and zero at the edges, /32-36/.

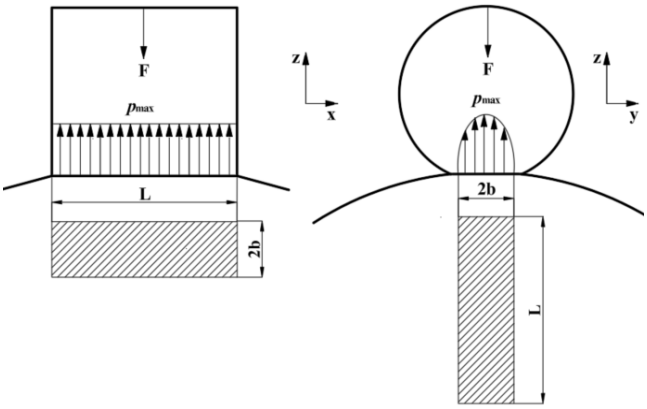


Figure 2. Line contact.

The total radial applied load F on the contact patch is equal to the volume of the half-prism as follows:

$$F = \frac{1}{2}\pi a L p_{\max}, \tag{1}$$

where: L is length of the contact along the cylinder axis.
The maximum pressure can be solved as follows:

$$p_{\max} = \frac{2F}{\pi a L}. \tag{2}$$

The average pressure is the applied force divided by the contact-patch area:

$$p_{avg} = \frac{F}{A} = \frac{F}{2aL}. \quad (3)$$

The applied force, depending on the average pressure, is:

$$F = 2aLp_{avg}. \quad (4)$$

Then, the maximum pressure can be rearranged:

$$p_{\max} = \frac{4}{\pi} p_{avg} \cong 1.273 p_{avg}. \quad (5)$$

A cylindrical geometry constant can be defined depending on the radii R_1 and R_2 of the two cylinders:

$$\Re = \frac{1}{2}\left(\frac{1}{R_1} + \frac{1}{R_2}\right). \quad (6)$$

The contact-patch half-width a is calculated as:

$$a = \sqrt{\frac{2}{\pi}\frac{m_1 + m_2}{\Re}\frac{F}{L}}, \quad (7)$$

where: m_1 and m_2 are material constants as defined:

$$m_1 = \frac{1-\nu_1^2}{E_1}, \quad (8)$$

and

$$m_2 = \frac{1-\nu_2^2}{E_2}, \quad (9)$$

where: ν_1 and ν_2 are Poisson's ratios; and E_1 and E_2 are the Young's moduli of bearing parts materials.

Pressure distribution within the semi-elliptical prism is:

$$p = p_{\max}\sqrt{1 - \frac{x^2}{a^2}}. \quad (10)$$

Equations presented above for contact stresses assume that the load is pure rolling, that is, static. When rolling and sliding are both present and dynamic, the stress field is distorted by tangential loading. This is a combination of rolling contact with relatively low-velocity sliding, /32-36/.

Effect of a sliding component on the contact stress

The sliding load has a significant effect on the stress field. The stresses can be expressed as separate components, where one set is due to the normal load on the rollers and the other set is due to the tangential friction force. These are combined to obtain the complete stress situation, /32-36/.

Stresses due to the normal load $p_{\max}$ are given by following equations:

$$\sigma_{xn} = -\frac{z}{\pi}\left[\frac{a^2 + 2x^2 + 2z^2}{a}\beta - \frac{2\pi}{a} - 3xa\right]p_{\max}, \quad (11)$$

$$\sigma_{zn} = -\frac{z}{\pi}[a\beta - x\alpha]p_{\max}, \quad (12)$$

$$\tau_{xzn} = -\frac{1}{\pi}z^2\alpha p_{\max}. \quad (13)$$

Stresses for the frictional unit force $f_{\max}$ are given by the following equations:

$$\sigma_{xt} = -\frac{1}{\pi}\left[(2x^2 - 2a^2 - 3z^2)\alpha + 2\pi\frac{x}{a} + 2(a^2 - x^2 - z^2)\frac{x}{a}\beta\right]f_{\max} \quad (14)$$

$$\sigma_{zt} = -\frac{1}{\pi}z^2\alpha f_{\max}, \quad (15)$$

$$\tau_{xzt} = -\frac{1}{\pi}\left[(a^2 + 2x^2 + 2z^2)\frac{z}{a}\beta - 2\pi\frac{z}{a} - 3xz\alpha\right]f_{\max}, \quad (16)$$

where: factors α and β are given by following equations:

$$\alpha = \frac{\pi}{k_1}\frac{1 - \sqrt{\frac{k_2}{k_1}}}{\sqrt{\frac{k_2}{k_1}}\sqrt{2\sqrt{\frac{k_2}{k_1}} + \left(\frac{k_1 + k_2 - 4a^2}{k_1}\right)}}, \quad (17)$$

$$\beta = \frac{\pi}{k_1}\frac{1 + \sqrt{\frac{k_2}{k_1}}}{\sqrt{\frac{k_2}{k_1}}\sqrt{2\sqrt{\frac{k_2}{k_1}} + \left(\frac{k_1 + k_2 - 4a^2}{k_1}\right)}}, \quad (18)$$

$$k_1 = (a + x)^2 + z^2, \quad (19)$$

$$k_1 = (a - x)^2 + z^2. \quad (20)$$

The tangential unit force $f_{\max}$ is calculated from the normal load and coefficient of friction μ, and is written as follows:

$$f_{\max} = \mu p_{\max}. \quad (21)$$

The independent variables are the coordinates x and z in the cross section of the roller in reference to the contact point, the half-width a of the contact patch, and maximal normal load $p_{\max}$ at the contact point.

The above equations define the behaviour of the stress functions below the surface, but when $z = 0$, the factors α and β become infinite, and these equations fail. Other forms of the equations are needed to account for the stresses on the surface of the contact patch.

When $z = 0$: if $|x| \le a$ then

$$\sigma_{xn} = -p_{\max}\sqrt{1 - \frac{x^2}{a^2}} \quad \text{else} \quad \sigma_{xn} = 0, \sigma_{zn} = \sigma_{xn}, \tau_{xzn} = 0 \quad (22)$$

When $|x| \ge a$, then $\sigma_{xt} = -2f_{\max}\left(\frac{x}{a} - \sqrt{\frac{x^2}{a^2} - 1}\right)$ (23)

When $|x| \le -a$, then $\sigma_{xt} = -2f_{\max}\left(\frac{x}{a} + \sqrt{\frac{x^2}{a^2} - 1}\right)$ (24)

When $|x| \le a$, then $\sigma_{xt} = -2f_{\max}\frac{x}{a}$, $\sigma_{zt} = 0$ (25)

When $|x| \le a$, then $\tau_{xzt} = -f_{\max}\sqrt{1 - \frac{x^2}{a^2}}$ else $\tau_{xzt} = 0$. (26)

The total stress on each Cartesian plane is calculated by superposing the components for normal and tangential loads:

$$\sigma_x = \sigma_{xn} + \sigma_{xt}, \quad (27)$$

$$\sigma_z = \sigma_{zn} + \sigma_{zt}, \quad (28)$$

$$\tau_{xz} = \tau_{xzn} + \tau_{xzt}. \quad (29)$$

The stress field can be two-dimensional for a very short roller. For short rollers, σ_y is zero, and they are assumed to be in the plane stress condition. If the rollers are axially long, then a plane strain condition will exist in the region away from the ends, producing a three-dimensional stress state. The stress in the y direction can be written as follows:

$$\sigma_y = \nu(\sigma_x + \sigma_z), \quad (30)$$

where: ν is Poisson's ratio.

Von Mises effective stress

It is often convenient in situations involving combined tensile and shear stresses acting on the same point to define

an effective stress. The distortion-energy approach provides a good means to do this for ductile materials.

The Von Mises effective stress σ_{VM} is defined as the uniaxial tensile stress that would create the same distortion energy as is created by the actual combination of applied stresses. This approach allows us to treat cases of combined, multiaxial tension and shear stresses as if they were due to pure tensile loading.

The Von Mises effective stress σ_{VM} for the three-dimensional case, by using principal stresses, is:

$$\sigma_{VM}=\sqrt{\sigma_1^2+\sigma_2^2+\sigma_3^2-\sigma_1\sigma_2-\sigma_2\sigma_3-\sigma_1\sigma_3}\,. \quad (31)$$

For the two-dimensional case, the Von Mises effective stress σ_{VM} is:

$$\sigma_{VM}=\sqrt{\sigma_1^2-\sigma_1\sigma_3+\sigma_3^2}\,. \quad (32)$$

The Von Mises effective stress σ_{VM} for the three-dimensional case can be expressed in terms of applied stresses, and is:

$$\sigma_{VM}=\sqrt{\frac{(\sigma_x-\sigma_y)^2+(\sigma_y-\sigma_z)^2}{2}+\frac{(\sigma_z-\sigma_x)^2+6(\tau_{xy}^2+\tau_{yz}^2+\tau_{zx}^2)}{2}} \quad (33)$$

If expressed in terms of applied stresses, the Von Mises effective stress σ_{VM} is:

$$\sigma_{VM}=\sqrt{\sigma_x^2+\sigma_y^2-\sigma_x\sigma_y+3\tau_{xy}^2}\,. \quad (34)$$

Alternating and mean components

The Von Mises effective stresses for alternating and mean components are calculated for a triaxial stress state using the following form of Von Mises stress:

$$\sigma_a^1=\sqrt{\frac{(\sigma_{xa}-\sigma_{ya})^2+(\sigma_{ya}-\sigma_{za})^2+(\sigma_{za}-\sigma_{xa})^2}{2}+\frac{6(\tau_{xya}^2+\tau_{yza}^2+\tau_{zxa}^2)}{2}}\,, \quad (35)$$

where: σ_a is alternating stress.

$$\sigma_m^1=\sqrt{\frac{(\sigma_{xm}-\sigma_{ym})^2+(\sigma_{ym}-\sigma_{zm})^2+(\sigma_{zm}-\sigma_{xm})^2}{2}+\frac{6(\tau_{xym}^2+\tau_{yzm}^2+\tau_{zxm}^2)}{2}}\,, \quad (36)$$

where: σ_m is mean stress.

For a biaxial stress case, the following form of the Von Mises stress is used:

$$\sigma_a^1=\sqrt{\sigma_{xa}^2+\sigma_{ya}^2-\sigma_{xa}\sigma_{ya}+3\tau_{xya}^2}\,, \quad (37)$$

$$\sigma_m^1=\sqrt{\sigma_{xm}^2+\sigma_{ym}^2-\sigma_{xm}\sigma_{ym}+3\tau_{xym}^2}\,. \quad (38)$$

BEARING FATIGUE LIFE ESTIMATION

In the available literature many scientists have made studies to calculate the fatigue life of bearings. However, standards such as ANSI and ISO are also available for bearing life calculations.

Some of the empirical equations and standardised calculation methods suggested in literature for rolling bearing life calculations are summarised below.

Lundberg and Palmgren developed a fatigue life estimation method for roller-raceway line contact, as /35, 36/:

$$L=\left(\frac{Q_C}{Q_e}\right)^4, \quad (39)$$

where: Q_C is basic dynamic load capacity of a raceway contact; and Q_e is equivalent rolling element load. Basic dynamic capacity Q_C is given by

$$Q_C=552\lambda\frac{(1\mp\gamma)^{29/27}}{(1\pm\gamma)^{1/4}}\left(\frac{\gamma}{\cos\alpha}\right)D^{29/27}l^{2/7}Z^{-1/4}, \quad (40)$$

where: λ is reduction factor; α is contact angle; D is roller diameter; l is effective roller length, and Z is the number of rolling elements per row.

Equivalent rolling element load Q_e is given by:

$$Q_e=\left(\frac{1}{Z}\sum_{j=1}^{j=Z}Q_j^4\right)^{1/4} \quad (41)$$

where: Z is number of rolling elements per row; and Q_j is the applied load.

Lundberg and Palmgren estimated that the fatigue life of roller bearing should be calculated by /35, 36/:

$$L=\left(\frac{C}{F_e}\right)^{10/3} \quad (42)$$

where: C is basic dynamic load capacity of a bearing raceway; and F_e is equivalent applied load. The equivalent applied load is given by

$$F_e=XF_r+YF_a\,, \quad (43)$$

where: X is radial load factor; F_r is applied radial load; Y is axial load factor; and F_a is applied axial load. Basic dynamic load capacity is given by

$$C=207\lambda\left\{1+\left[1.04\left(\frac{1-\gamma}{1+\gamma}\right)^{143/108}\right]^{9/2}\right\}^{-2/9}\frac{\gamma^{2/9}(1-\gamma)^{29/27}}{(1+\gamma)^{1/4}}\times \times(il\cos\alpha)^{7/9}Z^{3/4}D^{29/27}\,. \quad (44)$$

Based on Lundberg and Palmgren approaches and considering improved fatigue resistance of bearing materials, the ANSI standard offers an estimation for radial roller bearing as follows, /35, 36/:

$$C=f_{cm}(il\cos\alpha)^{7/9}Z^{3/4}D^{29/27}, \quad (45)$$

where: f_{cm} is the material factor; i is the number of rows.

For contact problems, the highest stresses usually occur below the surface. The fatigue life is calculated on the basis of subsurface stresses.

According to the stress-life theory, the fatigue life or number of stress cycles to failure N is calculated by Basquin's equations as follows:

$$N=\left(\frac{\sigma_{VM}}{2^b S_f'}\right)^{1/b}, \quad (46)$$

where: σ_{VM} is equivalent Von Mises fatigue stress; b is fatigue strength exponent; and S_f' is fatigue strength coefficient.

NUMERICAL EXAMPLE

The stress-life theory with Basquin's equations is employed during simulation. A radial roller bearing is considered in the numerical example. The contact pressure, Von Mises stress and fatigue life of roller bearings are calculated based on geometrical parameters, material parameters and loading parameters by using the MATLAB® programme. A flow chart of the calculation algorithm is shown in Fig. 3.

The algorithm calculates the fatigue life of a rolling bearing based on the input parameters. For each set of inputs, the calculated fatigue life is compared with the required life; if the bearing meets the criteria, the process stops; otherwise, it continues with adjusted parameters. The roller bearing is shown in Fig. 4.

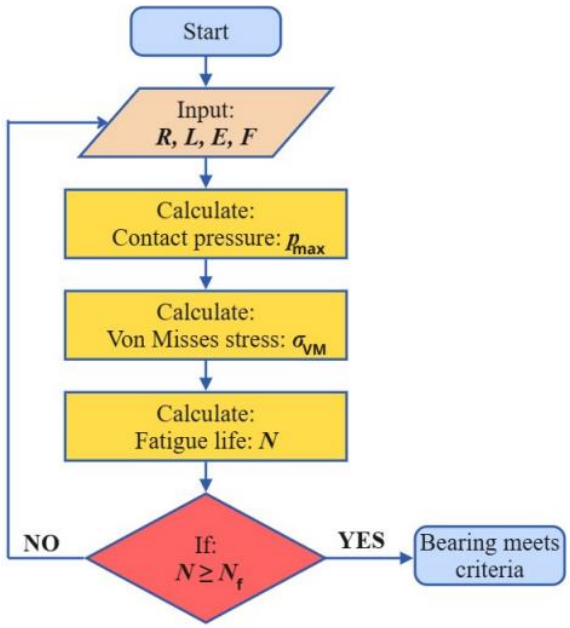


Figure 3. Flow chart of fatigue life calculation of a roller bearing.

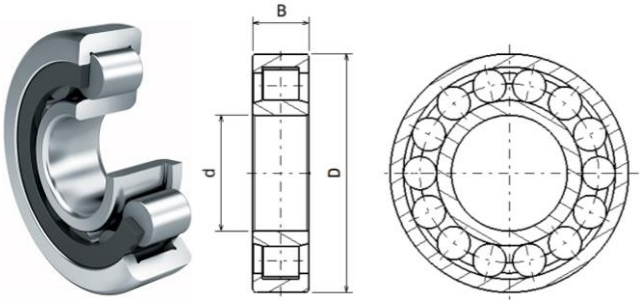


Figure 4. Roller bearing.

Data for calculating maximum pressure, Von Mises stress and fatigue life are: elasticity modulus of materials E_1 = (180000…210000) N/mm^2 and E_2 = 210000 N/mm^2; Poisson's ratio ν = 0.28; applied load F = (500…2500) N; roller length L = (10…40) mm; roller radius R_1 = (4…10) mm and raceway radius R_2 = 40 mm; the material is considered to be 1045 steel with a material coefficient of b = –0.074.

The effects of roller radius R_1 on the maximum pressure, von Mises stress, and fatigue life, for R_2 = 40 mm, l = 10 mm, E_1 = E_2 = 210000 N/mm^2, and F = 500 N, are presented in Table 1.

The maximum contact pressure p_{max} obtained by varying the roller element radius R_1 relation is shown in Fig. 5. Increasing the roller element radius R_1 results in a reduction in the maximum contact pressure p_{max}.

The Von Mises stress σ_{VM} obtained by varying the roller element radius R_1 relation is shown in Fig. 6. Increasing the roller element radius R_1 results in a reduction in Von Mises stress σ_{VM}.

Table 1. Effects of the roller element radius R_1.

No	R_1 /mm/	a /mm/	A /mm^2/	p_{max} /N/mm^2/	σ_{VM} /N/mm^2/	N /cycle/
1	4.000	0.045	0.902	706.155	596.648	$248 \cdot 10^6$
2	4.667	0.048	0.967	658.706	556.558	$636 \cdot 10^6$
3	5.333	0.051	1.026	620.745	524.483	$1418 \cdot 10^6$
4	6.00	0.054	1.080	589.531	498.110	$2848 \cdot 10^6$
5	6.667	0.056	1.130	563.316	475.961	$5266 \cdot 10^6$
6	7.333	0.059	1.177	540.924	457.041	$9110 \cdot 10^6$
7	8.00	0.061	1.221	521.530	440.654	$14921 \cdot 10^6$
8	8.667	0.063	1.262	504.537	426.297	$23346 \cdot 10^6$
9	9.3337	0.065	1.300	489.503	413.594	$35136 \cdot 10^6$
10	10.0007	0.067	1.337	476.089	402.260	$51147 \cdot 10^6$

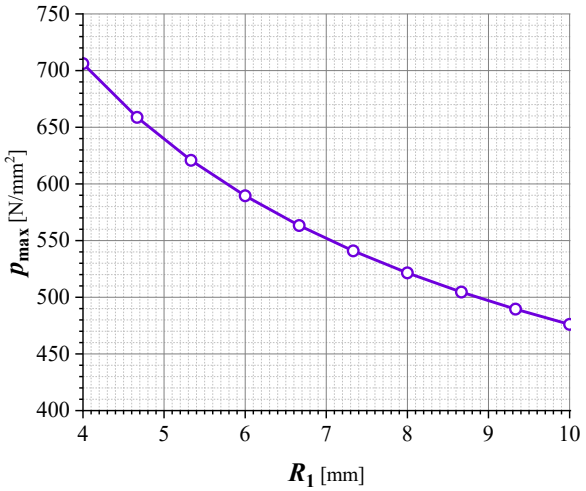


Figure 5. Maximum contact pressure with varying roller radius.

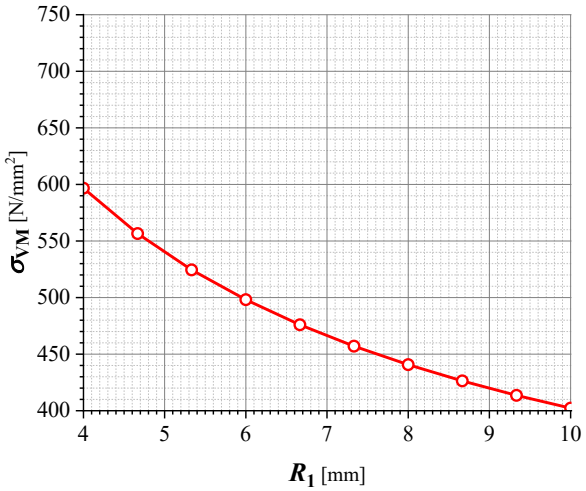


Figure 6. Von Mises stress with varying roller radius.

The fatigue life N obtained by varying the roller radius R_1 relation is shown in Fig. 7. Increasing the roller element radius R_1 results in an increase in the fatigue life N.

The effect of the roller element length L on the maximal contact pressure, Von Mises stress and fatigue life, for R_1 = 6 mm, R_2 = 40 mm, $E1$ = $E2$ = 210000 N/mm^2, and F = 500 N, is given in Table 2.

The maximum contact pressure p_{max} obtained by varying the roller element length L relation is shown in Fig. 8. Increasing the roller element length L results in a reduction in maximum contact pressure p_{max}.

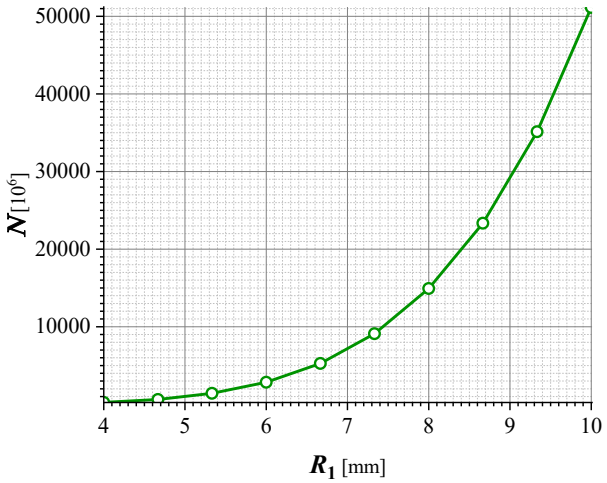


Figure 7. Fatigue life with varying roller radius.

Table 2. Effects of roller length L.

No	L /mm/	a /mm/	A /mm²/	p_{max} /N/mm²/	σ_{VM} /N/mm²/	N /cycle/
1	10.000	0.054	1.080	589.531	498.110	$3 \cdot 10^9$
2	13.333	0.047	1.247	510.549	431.376	$20 \cdot 10^9$
3	16.667	0.042	1.394	456.649	385.834	$90 \cdot 10^9$
4	20.000	0.038	1.527	416.862	352.217	$308 \cdot 10^9$
5	23.333	0.035	1.650	385.939	326.090	$873 \cdot 10^9$
6	26.667	0.033	1.763	361.013	305.029	$2151 \cdot 10^9$
7	30.000	0.031	1.870	340.366	287.584	$4768 \cdot 10^9$
8	33.333	0.030	1.972	322.900	272.826	$9716 \cdot 10^9$
9	36.667	0.028	2.068	307.873	260.130	$18500 \cdot 10^9$
10	40.000	0.027	2.160	294.766	249.055	$33304 \cdot 10^9$

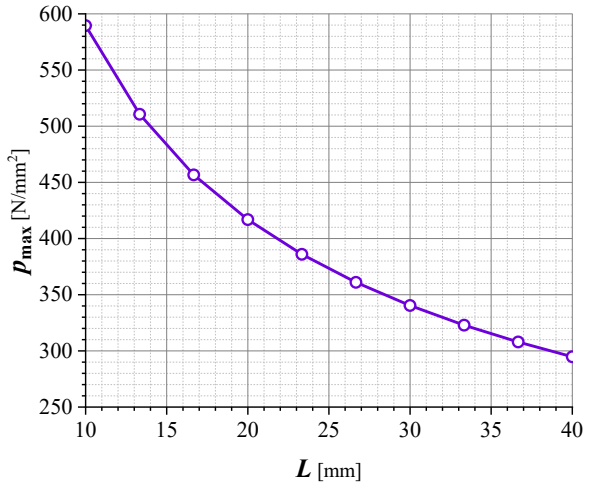


Figure 8. Maximum contact pressure with varying roller length.

The Von Mises stress σ_{VM} obtained by varying the roller element length L relation is shown in Fig. 9. Increasing the roller element length L results in a reduction in Von Mises stress σ_{VM}.

The fatigue life N obtained by varying the roller element length L relation is shown in Fig. 10. Increasing the roller element length L results in an increase in fatigue life N.

The effects of the roller material elasticity modulus E_1 on the maximum contact pressure, Von Mises stress and fatigue life, for $E_2 = 210000$ N/mm²; $R_1 = 6$ mm, $R_2 = 40$ mm, $L = 10$ mm, and $F = 500$ N is given in Table 3.

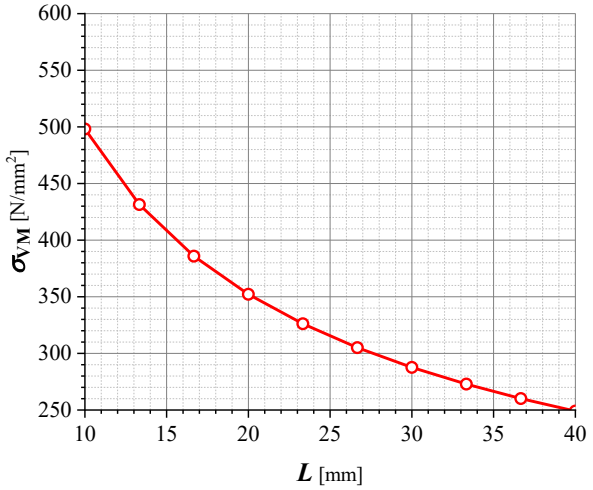


Figure 9. Von Mises stress with varying roller length.

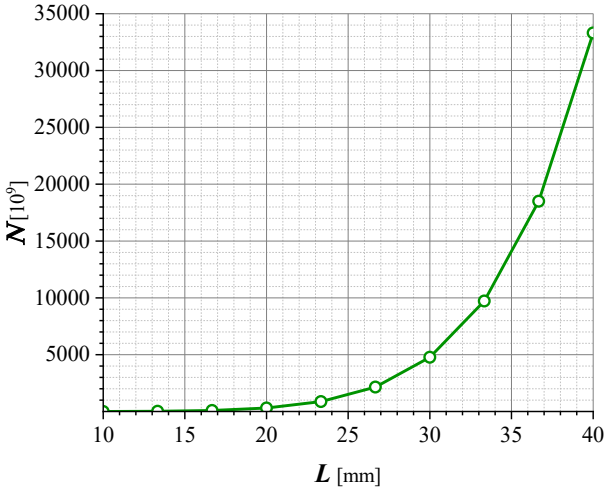


Figure 10. Fatigue life with varying roller length.

Table 3. Effects of roller element elasticity modulus E_1.

No	E_1 /N/mm²/	a /mm/	A /mm²/	p_{max} /N/mm²/	σ_{VM} /N/mm²/	N /cycle/
1	180000	0.056	1.124	566.403	478.569	$48910 \cdot 10^5$
2	182220	0.056	1.120	568.272	480.148	$46780 \cdot 10^5$
3	184440	0.056	1.117	570.114	481.704	$44779 \cdot 10^5$
4	186670	0.056	1.113	571.929	483.238	$42896 \cdot 10^5$
5	188890	0.056	1.110	573.719	484.750	$41123 \cdot 10^5$
6	191110	0.055	1.106	575.483	486.240	$39452 \cdot 10^5$
7	193330	0.055	1.103	577.222	487.710	$37875 \cdot 10^5$
8	195560	0.055	1.100	578.938	489.159	$36386 \cdot 10^5$
9	197780	0.055	1.096	580.629	490.589	$34980 \cdot 10^5$
10	200000	0.055	1.093	582.297	491.998	$33649 \cdot 10^5$

The maximum contact pressure p_{max}, Von Mises stress σ_{VM}, and fatigue life N obtained by varying the roller elasticity modulus E_1 are shown in Figs. 11-13.

Increasing the roller element elasticity modulus E_1 results in an increase of p_{max} and σ_{VM}. Increasing the roller element elasticity modulus E_1 results in a reduction of fatigue life N. The effects of the applied load F on the maximum contact pressure, Von Mises stress and fatigue life, for $R_1 = 6$ mm, $R_2 = 40$ mm, $L = 10$ mm, and $E_1 = E_2 = 210000$ N/mm², are given in Table 4.

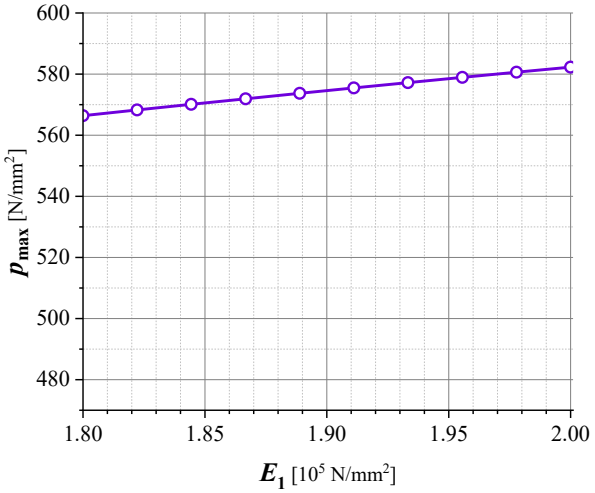


Figure 11. Contact pressure with varying roller elasticity modulus.

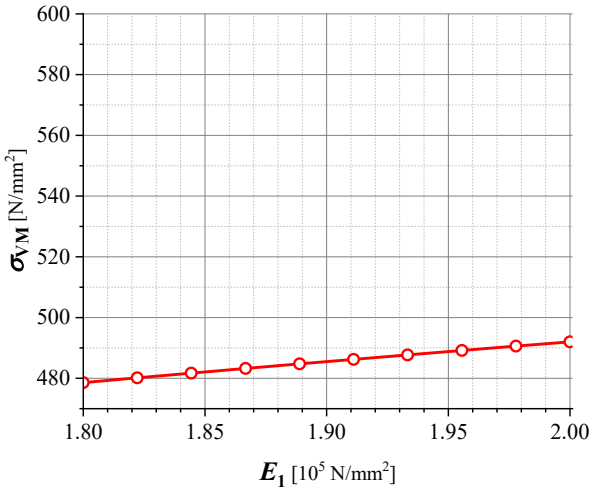


Figure 12. Von Mises stress with varying roller elasticity modulus.

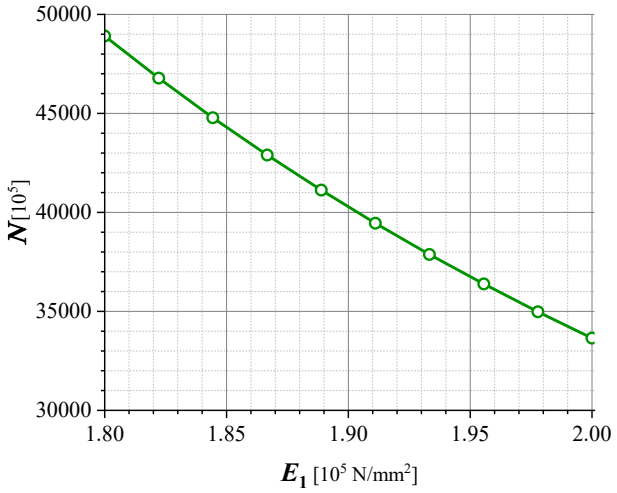


Figure 13. Fatigue life with varying roller elasticity modulus.

Table 4. Effects of the applied load.

No	F /N/	a /mm/	A /mm^2/	p_{max} /N/mm^2/	σ_{VM} /N/mm^2/	N /cycle/
1	500	0.054	1.080	589.500	498.100	$28479 \cdot 10^5$
2	722	0.065	1.527	833.700	704.400	$2374 \cdot 10^5$
3	944	0.074	1.870	1021.100	862.800	$387 \cdot 10^5$
4	1166	0.082	2.160	1179.100	996.200	$93 \cdot 10^5$
5	1388	0.090	2.415	1318.200	1113.800	$29 \cdot 10^5$
6	1611	0.097	2.645	1444.100	1220.100	$10 \cdot 10^5$
7	1833	0.103	2.857	1559.800	1317.900	$4 \cdot 10^5$
8	2055	0.110	3.054	1667.400	1408.900	$2 \cdot 10^5$
9	2277	0.115	3.240	1768.600	1494.300	$1 \cdot 10^5$
10	2500	0.121	3.415	1864.300	1575.200	$1 \cdot 10^5$

The maximum contact pressure p_{max} and Von Mises stress σ_{VM} obtained by varying the applied load relation are shown in Figs. 14 and 15. Increasing the applied load F results in an increase in p_{max} and σ_{VM}.

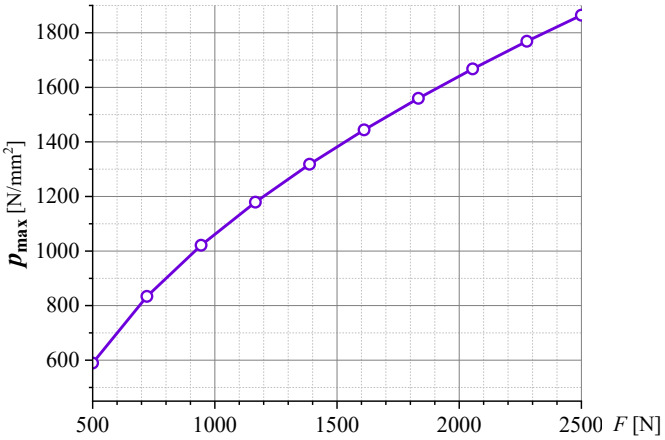


Figure 14. Maximum contact pressure with varying applied load.

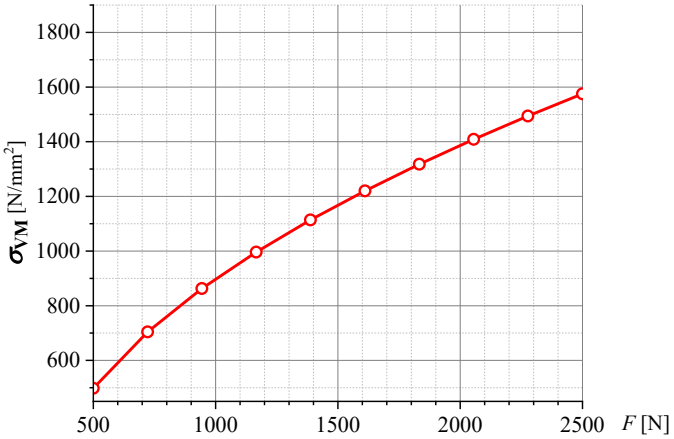


Figure 15. Von Mises stress with varying applied load.

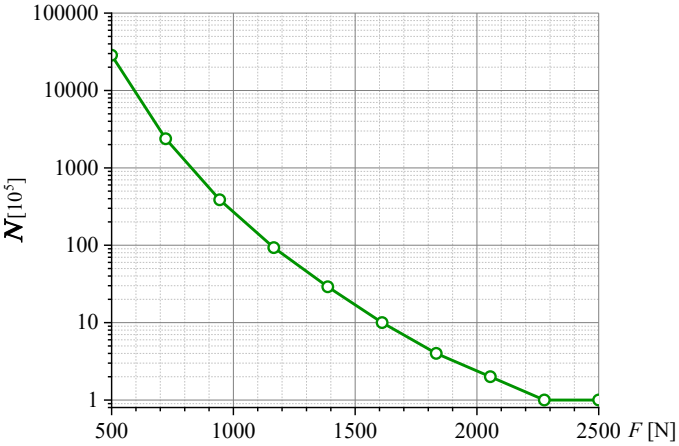


Figure 16. Fatigue life with varying applied load.

The fatigue life N obtained by varying the applied load F relation is shown in Fig. 16. Increasing the applied load F results in a reduction in fatigue life *N*.

DISCUSSION

Comparison of parameter effectiveness on contact pressure, Von Mises stress and fatigue life in cylindrical roller bearings are presented in Table 3.

Table 3. Influence of design and loading parameters on contact pressure, von Mises stress, and fatigue life.

Parameters/effects		Contact pressure	Von Mises stress	Fatigue life
Roller element radius R	↗	↘	↘	↗
Roller element length L	↗	↘	↘	↗
Roller element elasticity modulus E	↗	↗	↗	↘
Applied load F	↗	↗	↗	↘

This study aims to obtain a computational model for the lifetime estimation of cylindrical roller bearings. For this objective, the maximum contact pressure, equivalent static Von Mises stress, and equivalent dynamic Von Mises stress are calculated. The influence of effective parameters such as geometrical parameters, material parameters, and working parameters on the fatigue failure of rolling bearings is simulated. Equivalent dynamic Von Mises stresses are determined. The life of cylindrical roller bearings is estimated by using Basquin's equation. Thus, the influence of geometric, material, and loading parameters on the fatigue life of cylindrical roller bearings is evaluated.

The numerical results demonstrate a clear dependence of contact stresses and fatigue life on the considered geometry, material, and loading parameters. Variations in roller geometry, particularly the roller radius and length, significantly affect the contact conditions by modifying the contact area and stress distribution along the line contact. An increase in these geometric parameters leads to reduced maximum contact pressure and equivalent von Mises stress, which in turn contributes to an extended fatigue life. These trends are consistent with classical contact mechanics principles and confirm the importance of appropriate geometric design in cylindrical roller bearings.

Effects of geometric parameters on the fatigue life of cylindrical roller bearings are summarised as follows:

- Increasing the roller radius R_1 leads to a decrease in the maximum contact pressure p_{max} and in the equivalent Von Mises stress σ_{VM}, while simultaneously extending the fatigue life *N*. This behaviour is attributed to a reduced contact path radius and a smaller contact area.
- Increasing the roller length *L* similarly causes reductions in both p_{max} and σ_{VM}, resulting in a longer fatigue life *N*, due to the enlarged contact line and modified stress distribution along the roller.

Material properties are also shown to play a crucial role in fatigue behaviour:

- An increase in the roller element elastic modulus E_1 causes higher maximum contact pressure and higher equivalent Von Mises stress σ_{VM}, while reducing the fatigue life *N*, due to a smaller effective contact area.

The results indicate that higher elastic modulus values increase contact stiffness, resulting in elevated contact pressures and stress levels. Consequently, bearings manufactured from stiffer materials exhibit a reduced fatigue life under identical loading conditions. This highlights the necessity of considering material elasticity together with geometric design, rather than treating material selection as a secondary design step.

Furthermore, the influence of external loading is found to be dominant, as increased applied loads directly intensify contact stresses and accelerate fatigue damage accumulation.

- Increasing the applied *F* results in an increase in maximal contact pressure p_{max}, an increase in the Von Mises stress σ_{VM} and a reduction in fatigue life *N*.

The presented results underline the strong interaction between geometry, material properties, and operating conditions, and demonstrate that reliable fatigue life estimation of roller bearings requires their simultaneous consideration within a unified computational framework.

Bearing designers and manufacturers should aim to maximise key geometric dimensions, such as roller radius and length, while selecting materials with appropriate elasticity to enhance bearing performance. Reliability-based analyses are essential to provide probabilistic assessments for new products, ensuring that the predicted service life meets requirements and strengthening the manufacturer's reputation on the market. Additionally, optimisation studies are required to satisfy specific design and loading conditions; such approaches will be further explored and experimentally validated in future work.

CONCLUSIONS

The study presents a computational framework for estimating the fatigue life of roller bearings under realistic loading conditions. The proposed methodology integrates contact pressure evaluation, equivalent von Mises stress analysis, and fatigue life prediction based on rolling contact fatigue principles.

The main scientific contribution of this work lies in the systematic assessment of the influence of geometric, material, and loading parameters on bearing fatigue life, enabling the identification of parameter ranges that promote reduced contact stresses and extended service life. Results indicate that bearing fatigue performance cannot be reliably assessed by geometric parameters alone but requires the combined consideration of material properties and operating loads.

The developed approach improves the conventional life estimation procedure by providing a physically grounded and numerically supported basis for bearing design and parameter selection. The presented findings contribute to more reliable fatigue life prediction of cylindrical roller bearings and support further developments toward optimisation-based and reliability-oriented bearing design.

ACKNOWLEDGEMENT

Contribution of authors T.L., P.Lj., and J.A. is supported by the Ministry of Science, Technological Development and Innovation, Republic of Serbia, Contract No. 451-03-34/2026-03/200105 and by COST Action CA23155 - A pan-European network of Ocean Tribology (OTC).

REFERENCES

1. Rusiński, E., Czmochowski, J., Moczko, P., Pietrusiak, D. (2016), *Challenges and strategies of long-life operation and maintenance of technical objects*, FME Trans. 44(3): 219-228. doi: 10.5937/fmet1603219R
2. Bakić, G., Đukić, M., Lazović, T., et al. (2007), *New methodology for monitoring and prevention of rotating parts failures*, FME Trans. 35(4): 195-200.
3. Azouzi, K., Kouadria, M., Dehar, K.E., Meliani, M.H. (2025), *Vibration analysis of induction motor for bearing faults detection using Esprit method*, Struct. Integr. Life, 25(1): 141-146. doi: 10.69644/ivk-2025-01-0141
4. Lazović, T., Ljubojević, P., Stojanović, M. (2025), *Influence of lubricant contamination on ball bearing rating life*, Struct. Integr. Life, 25(2): 213-220. doi: 10.69644/ivk-2025-02-0213
5. Lazović, T., Marinković, A., Atanasovska, I., et al. (2024), *From innovation to standardization - A century of rolling bearing life formula*, Machines, 12(7): 444. doi: 10.3390/machines12070444
6. Lazović, T., Marinković, A., Popović, V. (2021), *Influence of load and design conditions on lubricant film thickness in the deep groove ball bearing*, J Chin. Soc. Mech. Eng. 42(4): 381-392.
7. Kim, T., Suh, J., Lee, J., et al. (2023), *Fatigue life prediction of double-row tapered roller bearings considering thermal effect*, Adv. Mech. Eng. 15(2): 168781322311540. doi: 10.1177/16878132231154099
8. Morales-Espejel, G.E., Misiaszek, M., Lengagne, T., Guo, L. (2024), *Durability of aircraft gas turbine mainshaft ball bearing applying surface and subsurface survival*, Tribol. Online, 19(6): 573-583. doi: 10.2474/trol.19.573
9. Allmaier, H. (2022), *Increase service life for rail wheel bearings - A review of grease lubrication for this application*, Lubricants, 10(3): 36. doi: 10.3390/lubricants10030036
10. Sadeghi, F., Jalalahmadi, B., Slack, T.S., et al. (2009), *A review of rolling contact fatigue*, J Tribol. 131(4): 041403. doi: 10.1115/1.3209132
11. Potočnik, R., Göncz, P., Flasker, J., Glodež, S. (2010), *Fatigue life of double row slewing ball bearing with irregular geometry*, Proc. Eng, 2(1): 1877-1886. doi: 10.1016/j.proeng.2010.03.202
12. Gönz, P., Potočnik, R., Glodež, S. (2011), *Load capacity of a three-row roller slewing bearing raceway*, Procedia Eng, 10: 1196-1201. doi: 10.1016/j.proeng.2011.04.199
13. Glodež, S., Potočnik, R., Flašker, J. (2012), *Computational model for calculation of static capacity and lifetime of large slewing bearing's raceway*, Mech. Mach. Theory, 47: 16-30. doi: 10.1016/j.mechmachtheory.2011.08.010
14. Potočnik, R., Göncz, P., Glodež, S. (2013), *Static capacity of a large double row slewing ball bearing with predefined irregular geometry*, Mech. Mach. Theory, 64: 67-79. doi: 10.1016/j.mechmachtheory.2013.01.010
15. Göncz, P., Drobne, M., Glodež, S. (2013), *Computational model for determination of dynamic load capacity of large three-row roller slewing bearings*, Eng. Fail. Anal, 32: 44-53. doi: 10.1016/j.engfailanal.2013.02.030
16. Göncz, P., Potočnik, R., Glodež, S. (2013), *Computational model for determination of static load capacity of three-row roller slewing bearings with arbitrary clearances and predefined raceway deformations*, Int. J. Mech. Sci, 73: 82-92. doi: 10.1016/j.ijmecsci.2013.04.012
17. Göncz, P., Ulbin, M., Glodež, S. (2015), *Computational assessment of the allowable static contact loading of a roller-slewing bearing's case-hardened raceway*, Int. J. Mech. Sci. 94-95: 174-184. doi: 10.1016/j.ijmecsci.2015.03.006
18. Lazović, T.M., Simonović, I.M., Marinković, A.B. (2022), *Service life of universally loaded deep groove ball bearing depending on internal clearance*. In: Rackov, M., Mitrović, R., Čavić, M. (Eds.), Machine and Industrial Design in Mechanical Engineering, KOD 2021. Mechanisms and Machine Science, 109: 121-129. Springer, Cham. doi: 10.1007/978-3-030-88465-9_9
19. Kunc, R., Žerovnik, A., Prebil, I. (2007), *Verification of numerical determination of carrying capacity of large rolling bearings with hardened raceway*, Int. J Fatigue, 29(9-11): 1913-1919. doi: 10.1016/j.ijfatigue.2007.02.003
20. Cui, Y., Su, Y. (2022), *Contact fatigue life prediction of rolling bearing considering machined surface integrity*, Industr. Lubr. Tribol. 74(1): 73-80. doi: 10.1108/ILT-08-2021-0345
21. Zhang, J., Shi, M., Du, X. (2025), *Surface defect initiation and evolution mechanism of the full-life-cycle rolling bearing and its vibration-based verification*, J Fail. Anal. Preven. 25: 1391-1407. doi: 10.1007/s11668-025-02216-5
22. Morales-Espejel, G.E., Gabelli, A., De Vries, A.J.C. (2015), *A model for rolling bearing life with surface and subsurface survival - tribological effect*, Tribol. Trans. 58(5): 894-906. doi: 10.1080/10402004.2015.1025932
23. Bozca, M. (2016), *Theoretical investigation of point contact for ball bearings application*, In: Proc. 57th Int. Conf. of Machine Design Departments - ICMD'2016, Zelezna Ruda, Plzen, pp. 195-200.
24. Bozca, M. (2021), *Effects of design parameters on static equivalent stress of radial rolling bearings*, Acta Polytechnica, 61(1): 163-173. doi: 10.14311/AP.2021.61.0163
25. Bozca, M. (2011), *Theoretical investigation of line contact for roller bearings application*, In: Proc. 57th Int. Conf. of Machine Design Departments - ICMD'2016, Zelezna Ruda, Plzen, pp. 201-206.
26. Ivannikov, V., Leontiev, M., Degtyarev, S., Popov, V. (2021), *Analysis of radial roller bearing rating life in complex loading conditions*, J Tribol. 144(3): 031201. doi: 10.1115/1.4051201
27. Ge, X., Zhang, C., Zhang, W., et al. (2025), *A nonlinear fatigue damage accumulation model for rolling bearing life prediction considering coupled load-variation effects*, Int. J Damage Mech. 35(2): 293-323. doi: 10.1177/10567895251358415
28. Zhao, H., Liu, H., Jin, Y., et al. (2021), *Feature extraction for data-driven remaining useful life prediction of rolling bearings*, IEEE Trans. Instrum. Meas. 70: 3511910. doi: 10.1109/TIM.2021.3059500
29. Liu, X., Zhang, Z., Li, Z., et al. (2025), *Advancements in bearing health monitoring and remaining useful life prediction: techniques, challenges, and future directions*, Meas. Sci. Technol. 36(3): 032003. doi: 10.1088/1361-6501/adafc8
30. Xue, B., Li, Y., Xu, Z., Chen, L. (2025), *Remaining useful life prediction for rolling bearing based on a hybrid data-driven method integrating similarity analysis*, Meas. Sci. Technol. 36 (9): 096217. doi: 10.1088/1361-6501/ae0809
31. Jiang, L., Cao, B., Zhang, X., et al. (2024), *A novel spatio-temporal characteristic extraction network for bearing remaining useful life prediction*, Meas. Sci. Technol. 35(11): 116142. doi: 10.1088/1361-6501/ad6f37
32. Norton, R.L., Machine Design - An Integrated Approach, 4th Ed., Pearson / Prentice Hall, Worcester, 2011.
33. Juvinal, R.C., Marshek, K.M., Fundamentals of Machine Component Design, John Wiley & Sons, New York, 2006.
34. Budynas, R.G., Nisbett, J.K., Shigley's Mechanical Engineering Design, 10th Ed., McGraw-Hill, New York, 2011.
35. Harris, T.A., Kotzalas, M.N., Essential Concepts of Bearing Technology, 5th Ed., CRC Press, Boca Raton, 2006.
36. Nguyen-Schafer, H., Computational Design of Rolling Bearings, 1st Ed., Springer, New York, 2016.

© 2026 The Author. Structural Integrity and Life, Published by DIVK (The Society for Structural Integrity and Life 'Prof. Dr Stojan Sedmak') (http://divk.inovacionicentar.rs/ivk/home.html). This is an open access article distributed under the terms and conditions of the Creative Commons Attribution-NonCommercial-NoDerivatives 4.0 International License